

Central Lancashire Online Knowledge (CLoK)

Title	Measurement of the Raman spectra and hygroscopicity of four pharmaceutical aerosols as they travel from pressurised metered dose inhalers (pMDI) to a model lung
Type	Article
URL	https://clock.uclan.ac.uk/16952/
DOI	https://doi.org/10.1016/j.ijpharm.2017.01.051
Date	2017
Citation	Davidson, N, Tong, H-J, Kalberer, M, Seville, Peter Craig, Ward, AD, Kuimova, MK and Pope, FD (2017) Measurement of the Raman spectra and hygroscopicity of four pharmaceutical aerosols as they travel from pressurised metered dose inhalers (pMDI) to a model lung. <i>International Journal of Pharmaceutics</i> , 520 (1-2). pp. 59-69. ISSN 0378-5173
Creators	Davidson, N, Tong, H-J, Kalberer, M, Seville, Peter Craig, Ward, AD, Kuimova, MK and Pope, FD

It is advisable to refer to the publisher's version if you intend to cite from the work.
<https://doi.org/10.1016/j.ijpharm.2017.01.051>

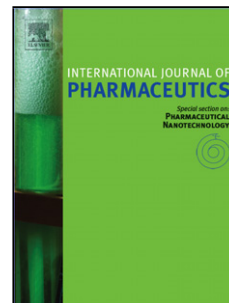
For information about Research at UCLan please go to <http://www.uclan.ac.uk/research/>

All outputs in CLoK are protected by Intellectual Property Rights law, including Copyright law. Copyright, IPR and Moral Rights for the works on this site are retained by the individual authors and/or other copyright owners. Terms and conditions for use of this material are defined in the <http://clock.uclan.ac.uk/policies/>

Accepted Manuscript

Title: Measurement of the Raman spectra and hygroscopicity of four pharmaceutical aerosols as they travel from pressurised metered dose inhalers (pMDI) to a model lung

Authors: N. Davidson, H.-J. Tong, M. Kalberer, P.C. Seville, A.D. Ward, M.K. Kuimova, F.D. Pope



PII: S0378-5173(17)30060-1
DOI: <http://dx.doi.org/doi:10.1016/j.ijpharm.2017.01.051>
Reference: IJP 16383

To appear in: *International Journal of Pharmaceutics*

Received date: 24-10-2016
Revised date: 12-1-2017
Accepted date: 25-1-2017

Please cite this article as: Davidson, N., Tong, H.-J., Kalberer, M., Seville, P.C., Ward, A.D., Kuimova, M.K., Pope, F.D., Measurement of the Raman spectra and hygroscopicity of four pharmaceutical aerosols as they travel from pressurised metered dose inhalers (pMDI) to a model lung. *International Journal of Pharmaceutics* <http://dx.doi.org/10.1016/j.ijpharm.2017.01.051>

This is a PDF file of an unedited manuscript that has been accepted for publication. As a service to our customers we are providing this early version of the manuscript. The manuscript will undergo copyediting, typesetting, and review of the resulting proof before it is published in its final form. Please note that during the production process errors may be discovered which could affect the content, and all legal disclaimers that apply to the journal pertain.

1 **Measurement of the Raman spectra and hygroscopicity of four pharmaceutical aerosols as they**
2 **travel from pressurised metered dose inhalers (pMDI) to a model lung**

3
4 N. Davidson^a, H. -J. Tong^b, M. Kalberer^b, P. C. Seville^{c,d}, A. D. Ward^e, M. K. Kuimova^f and F. D. Pope^{a*}

5 ^aSchool of Geography, Earth and Environmental Sciences, University of Birmingham, Edgbaston,
6 Birmingham, B15 2TT, UK.

7
8 ^bDepartment of Chemistry, University of Cambridge, Lensfield Road, Cambridge, CB2 1EW, UK.

9
10 ^cSchool of Pharmacy, University of Birmingham, Edgbaston, Birmingham, B15 2TT, UK.

11
12 ^dSchool of Pharmacy and Biomedical Sciences, University of Central Lancashire, Preston, Lancs,
13 PR1 2HE, UK.

14
15 ^eCentral Laser Facility, Rutherford Appleton Laboratory, Harwell, Oxford, OX11 0QX, UK.

16
17 ^fImperial College London, South Kensington Campus, London, SW7 2AZ, UK

18
19
20 *Corresponding author

21 Dr Francis Pope

22 School of Geography, Earth and Environmental Sciences, University of Birmingham, Edgbaston,
23 Birmingham, B15 2TT, UK.

24 f.pope@bham.ac.uk

25 Telephone – (+44) 0121 4149067

26
27 Key Words

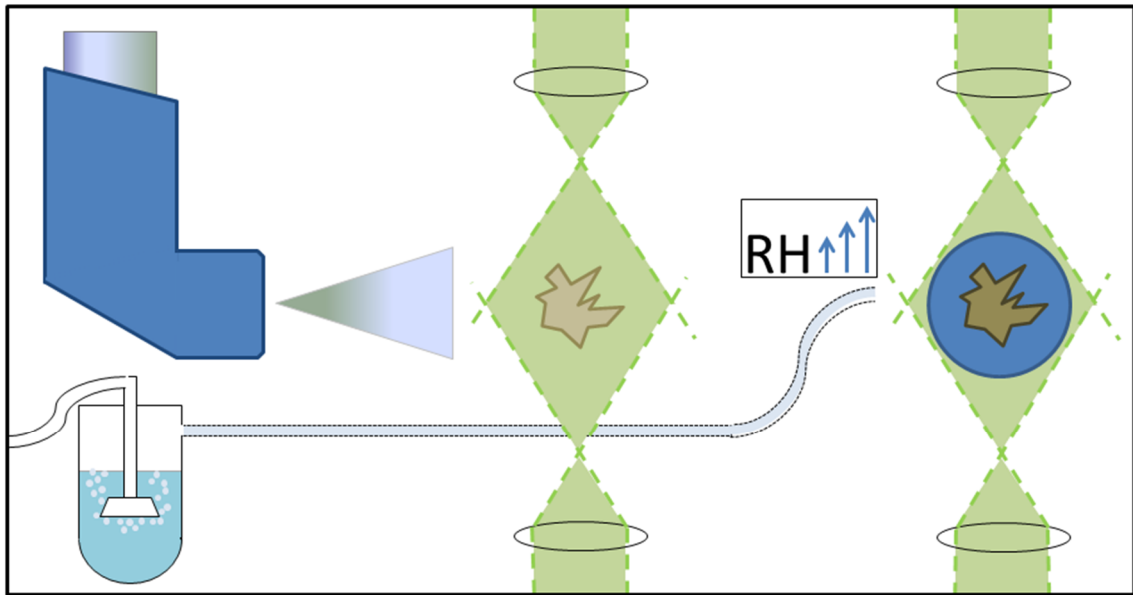
28
29 Hygroscopicity; optical trapping; laser tweezers; suspended particle; pMDI

30
31 Chemical compounds studied in this article

32
33 Salbutamol sulfate (PubChem CID: 39859); salmeterol xinafoate (PubChem CID: 56801); fluticasone
34 propionate (PubChem CID: 444036); ciclesonide (PubChem CID: 6918155)

35
36 This work was funded by the National Environmental Research Council
37 (Grant number: NE/L501712/1)

38
39
40 Graphical abstract



1

1 Abstract

2
3 Particle inhalation is an effective and rapid delivery method for a variety of pharmaceuticals,
4 particularly bronchodilation drugs used for treating asthma and COPD. Conditions of relative humidity
5 and temperature inside the lungs are generally very different from the outside ambient air, with the
6 lung typically being warmer and more humid. Changes in humidity, from inhaler to lung, can cause
7 hygroscopic phase transitions and particle growth. ~~Changing~~ Increasing particle size and mass can
8 negatively affect particle deposition within the lung leading to inefficient treatment, while
9 deliquescence prior to impaction is liable to accelerate drug uptake. To better understand the
10 hygroscopic properties of four pharmaceutical aerosol particles; pharmaceutical particles from four
11 commercially available pressurised metered dose inhalers (pMDIs) were stably captured in an optical
12 trap, and their composition was examined online via Raman spectroscopy. Micron-sized particles of
13 salbutamol sulfate, salmeterol xinafoate, fluticasone propionate and ciclesonide were levitated and
14 examined over a range of relative humidity values inside a chamber designed to mimic conditions
15 within the respiratory tract. The effect of temperature upon hygroscopicity was also investigated for
16 salbutamol sulfate particles. Salbutamol sulfate was found to have significant hygroscopicity,
17 salmeterol xinafoate showed some hygroscopic interactions, whilst fluticasone propionate and
18 ciclesonide revealed no observable hygroscopicity. Thermodynamic and structural modelling is used
19 to explain the observed experimental results.

21 1. Introduction

22 1.1 Respiratory drugs and drug delivery

23 Respiratory ailments in the form of asthma and Chronic Obstructive Pulmonary Disease (COPD) are
24 often managed with inhalable drugs. These drugs include beta-2 agonists such as salbutamol and
25 salmeterol, and corticosteroids like fluticasone and ciclesonide.

26 Salbutamol sulfate and salmeterol xinafoate are both *beta-2 adrenoceptor agonists*, meaning that
27 ~~they target the beta-2 receptors in bronchial muscle cells in a similar manner to adrenaline (Reisine,~~
28 ~~et al., 1983), forcing calcium out of the cells thus forcing them to relax, and opening the user's airways~~
29 ~~to allow easier breathing. Salbutamol (Ventalin™, Salamol™) has been a popular treatment for asthma~~
30 ~~and COPD since 1968 (Icha, 2007), while Salmeterol (Serevent™) was introduced in 1988 as a longer~~
31 ~~lasting alternative (Ullman & Svedmyr, 1988).~~

32 Fluticasone propionate (Flixotide™) is an artificial corticosteroid that assists breathing by reducing
33 inflammation in the lung lining (Harding, 1990)—Fluticasone propionate is also supplied as a
34 combination inhaler with salmeterol xinafoate (Seretide™) due to their complementary modes of
35 action (Woolcock, et al., 1996) (Chapman, et al., 1999) (Calverley, et al., 2003). Pure compounds rather
36 than mixtures were investigated in this study.

37 Ciclesonide (Alvesco™) is a recently developed inhaled corticosteroid used as a treatment for asthma,
38 hay fever and other respiratory ailments. ~~In order to reduce the mouth and throat infections~~
39 ~~associated with respiratory steroid application, ciclesonide is designed to be biologically inactive until~~
40 ~~it interacts with esterase enzymes present in the lung (Mutch, et al., 2007) at which point it is~~

1 hydrolysed to the active form desisobutryl-ciclesonide; these enzymes are not found in the oral cavity
2 to the same extent, and hence the potential benefit of reduced oropharyngeal side effects.

3 Inhalable drugs are predominately administered by nebuliser, dry powder inhaler (DPI) or by
4 pressurised metered dose inhaler (pMDI). Powdered nebulisers have been in use since the 19th century
5 (Sanders, 2007), while cheaper and more portable pMDIs were invented in 1955 (Purewal & Grant,
6 1997). The pMDI is now the most popular device for delivering drugs to the human respiratory system
7 in Great Britain and elsewhere (Lavorini, et al., 2011).

8 Modern pMDIs contain solid drug particles which are suspended in a liquefied hydrofluoroalkane
9 propellant: most commonly HFA-134a (Cripps, et al., 2000) (Leach, 2005). Other co-solvents such as
10 ethanol or oleic acid can be used depending on the drug (Bell & Newman, 2007). The solvent
11 rapidly evaporates within a few milliseconds at ambient temperature upon activation of the pMDI
12 (Stein, 2006), generating a fixed dose, inhalable aerosol of micron-sized solid drug particles travelling
13 at a wide range of planar velocities into the user's trachea and lungs (Crosland, et al., 2009).

14 **1.2 Significance of relative humidity and temperature on delivery efficiency**

15 Drugs acting within the respiratory tract are only effective if the particle aerodynamic diameters are
16 in the 1-5 μ m range since larger particles cannot reach the receptor sites inside the lungs (Labiris &
17 Dolovich, 2003). Hygroscopic particles can ~~change~~ increase in size and mass as they collect water from
18 the air (Broday & Georgopoulos, 2001) which means that particles manufactured in the ~~correct~~
19 size appropriate range when dry may swell to larger than optimal size and higher than optimal mass
20 by the time they pass through the moist air inside the trachea and ~~into~~ towards the lungs. While larger
21 particles are less likely to navigate to the regions where they can be absorbed most rapidly, more
22 massive particles have greater momentum, are more likely to impact the back of the throat than pass
23 into the lungs (Mansour, et al., 2016) and their direction of travel is less influenced by the Brownian
24 diffusion processes that would drive them to their intended destination (Tsuda, et al., 2013).

25 Previous work has shown (Tong, et al., 2014) that salbutamol sulfate deliquesces at around 92%
26 relative humidity (RH). Deliquescence describes the phase change of a crystalline solid to a saturated
27 solution droplet using water collected from the surrounding air. Temperature can affect the RH level
28 required to bring about deliquescence in hygroscopic substances but the effect varies between
29 compounds (Lipasek, et al., 2013). Temperature also has a significant influence over the saturation
30 vapour pressure of air (Lawrence, 2005) so the air inside the lungs at 37°C and near-100% RH contains
31 three times the concentration of water as outside air at similar RH and 20°C (Nave, 2004). However,
32 temperature influences the kinetics of drug dissolution only, rather than the thermodynamic
33 behaviour of solid particles, which remain relatively unchanged, and it is not expected to significantly
34 impact hygroscopic properties.

35 The rate of deliquescence dictates the rate of adsorption of drugs across lung epithelia, since a given
36 drug cannot be absorbed until it has fully dissolved (Bikiaris, 2011). This lends a time-critical aspect to
37 drug delivery since solid particles in the lungs are removed over time by ejection via the mucociliary
38 escalator in the ciliated regions of the lungs or partition into macrophages in the alveoli (Hardy &
39 Chadwick, 2000) and dissolution appears to be the rate-limiting step for the uptake of inhalable drugs
40 (Bur, et al., 2010). If more of a given drug is removed in these manners before it is fully dissolved, a

1 greater dose must be administered and the resultant side effects such as immunosuppression with
2 corticosteroids (Lee, et al., 2012) and hypoalkaemia with salbutamol (Hung, et al., 1999) will have
3 greater impacts on patient health.

4 On the other hand, as mentioned in the previous section rapid deliquescence can lead to an increase
5 in particle size that makes it more difficult for drugs to reach deep into the airways. Finding optimal
6 values for both particle size and hygroscopicity is important for providing patients with the most
7 efficiently delivered treatment with the least side effects, and is the primary motivation for this series
8 of experiments. Additionally, a better understanding of the hygroscopic properties of drug molecules
9 should inform which drugs are likely to be pre-wetted by the wicking effect of water uptake upon
10 inhalation, thus kick starting the dissolution of drug particles upon impaction onto higher respiratory
11 tract surfaces like the epithelium (Brain, et al., 2014).

12 Investigations are ongoing into the hygroscopic behaviour of drug aerosols delivered by nebuliser e.g.
13 (Haddrell, et al., 2014). However, the popularity of pMDI delivery for bronchodilation medication and
14 the logistical difficulties involved in modelling the pharmacokinetic behaviour of medication inside the
15 lung of a living creature mean that similar studies on pMDI-delivered drugs are justified. DPI
16 formulations have been shown to be vulnerable to high humidity conditions (Janson, et al., 2016) and
17 the lower particle velocity of DPI inhalations compared to pMDI (Ibrahim, et al., 2015) also implies
18 that high humidity conditions are potentially of even great concern for DPI devices. However, the
19 sudden change in humidity surrounding drug particles from both types of device upon inhalation mean
20 that changes to particles from pMDIs also merit attention.

21 It is worth noting that the lung deposition rate of pMDI-delivered material is normally less than 10%
22 (Newman, et al., 1981) and with optimised inhalation technique and additional equipment such as
23 spacers (Dolovich, et al., 1981) (Newman, 1996) maximum possible deposition appears to be around
24 25% of the total inhaled dose. Since larger particles are more likely to impact or be excluded by the
25 processes discussed above, concern over hygroscopic particle growth is justified.

26 This series of experiments investigates the use of an optical trap to stably levitate drug aerosols
27 released by popular pMDI devices and Raman spectroscopy to monitor signs of hygroscopic particle
28 growth upon rapid increase in RH. The set up allows for the control of temperature and RH to more
29 closely mimic the conditions inside the human lung than conventional cover slip analysis.

30

31 **2. Methods and Materials**

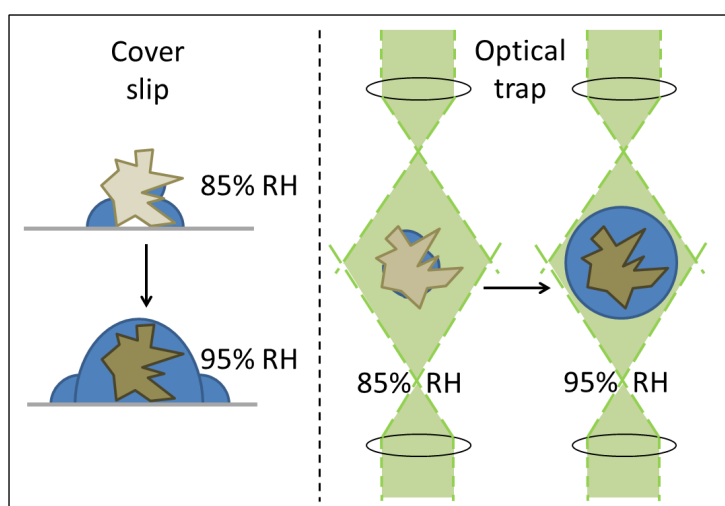
32 The combination of optical trap, Raman spectroscopy and model lung was first described in Tong et al
33 2014 (Tong, et al., 2014). The optical trap uses a counter propagating dual beam (CPDB) trap
34 configuration first described by Rkiouak et al. (Rkiouak, et al., 2014) and deployed in several
35 subsequent experiments (Tang, et al., 2014) (Jones, et al., 2015) (Hunt, et al., 2015). This trapping
36 setup is remarkable because it is capable of stably trapping micron-sized solid particles of non-
37 spherical geometry for periods of time up to several hours.

38

39 **2.1 Counter propagating dual beam optical trap**

1 The trapping beams were generated by a 1064 nm Nd:Yag laser (Ventus, Laser Quantum) passed
 2 through a beam splitter (Oz optics) and fibre-coupled into two single-mode fibres. Each fibre output
 3 was delivered to beam expansion and collimation optics before entering the objective lenses. The
 4 laser power at output was 15 mW from the top objective lens and 10 mW through the bottom
 5 objective lens (figure 2). The asymmetry in power ensured that trapped particles were driven closer
 6 to the optical focus plane of the bottom objective through which the Raman laser is passed, ensuring
 7 better focus on the resulting images (Rkiouak, et al., 2014). The foci of the lasers were positioned ~ 10
 8 μm apart, which created a trapping volume large enough to stably hold 1-5 μm particles for long
 9 periods. Once all useful observations had been collected from a trapped particle, the particle was
 10 allowed to fall under gravity to the cover slip by blocking the 1064 nm trapping beams.

11 There are several reasons to prefer an optical trap to cover slip analysis. The most significant is that
 12 pharmaceutical aerosols are, until they reach the respiratory tract, suspended particles and attempts
 13 to recreate their conditions should be as close as possible. Interactions between collecting substrates
 14 and water can measurably alter the deliquescence point of hygroscopic particles (Eom, et al., 2014)
 15 with surfaces like glass reducing the deliquescence point of sodium chloride by 1.5% compared to a
 16 suspended particle. Previous work in our group has also observed changes in particle efflorescence
 17 upon a cover slip compared to optical trap. Any particle landing on a cover slip will have part of its
 18 surface in contact with the cover slip rather than exposed to the surrounding air (see figure 1), so a
 19 hygroscopic particle will form a water layer beginning with a halo around the contact point with the
 20 cover slip rather than across the surface dictated by the particle's geometry and density of hygroscopic
 21 sites. The shape of the resulting droplet and rate of adsorption will both be affected by the presence
 22 of a cover slip.



23

24 Figure 1. An illustration of the influence of coverslips on the formation of water layers on
 25 hygroscopic particles. Optical trapping allows particles to remain suspended as they deliquesce in a manner
 26 more representative of particles *in vivo*.

27 This is especially important in time-critical experiments such as those reported in this paper. Optical
 28 trapping represents the best current option for making detailed observations of physical and chemical
 29 changes on suspended particles in varying conditions, and yields better resolved Raman spectra than
 30 particles observed on a cover slip due to the removal of interfering spectral features associated with
 31 the composition of the cover slip. Optical trapping is typically superior for single particle spectroscopy

1 when compared to other single particle levitation techniques, such as electrodynamic balances or
2 acoustic trapping, because the optical setup ensures good alignment between the studied particle and
3 spectroscopic probe (Hargreaves, et al., 2010).

4 Optical trapping is easiest with spherical or spheroidal particles and droplets due to their symmetry
5 (Ashkin, 1992). While the setup used in this work has demonstrated the capacity to trap non-spherical
6 particles for periods of an hour or longer (Rkiouak, et al., 2014) (Tong, et al., 2014), particles that are
7 closer to spheres are still easier to trap for the same reasons.

8 **2.2 Raman Spectroscopy**

9 Raman spectroscopy is a powerful technique for examining the functional groups and intermolecular
10 interactions of substances, requiring very small sample masses and no sample preparation (Hirschfeld
11 & Chase, 1986) (Vankeirsbilck, et al., 2002) and making it ideal for the analysis of micrometer-scale
12 drug particles. Raman spectroscopy has much lower signal-to-noise ratio than competing infrared
13 analysis techniques because of the visible range detection region, and because the scattering
14 wavelengths are separate from those of the excitation laser, so the technique can be effective with
15 very small samples whose absorption would be indistinguishable against a standard FT-IR beam
16 (PerkinElmer Inc, 2008). These experiments use a Raman setup which collects back-scattered photons
17 along the same path as the excitation laser, but filtering the excitation photons with a Razoredge
18 dichroic mirror and longpass edge filter combination (SemRock).

19 Raman scattering was generated using a 514.5nm Ar-ion laser (Innova 300C, Coherent), with a power
20 of 4.3mW measured at the laser focus. Each Raman spectrum was generated by a 30 second exposure
21 to the 514.5nm laser. This is longer than the residence time of particles in the respiratory system but
22 is necessary to generate usable and reproducible spectra. These wavelength and power settings were
23 selected based on previous experiments (Hunt, et al., 2013) as they were found to cause minimal
24 heating of samples over long periods of exposure. Raman scattered light was collected in the region
25 of 540-1830 cm^{-1} .

26 Wavelength calibration of the Raman spectrometer was carried out using a cover slip with raised sides
27 containing pure liquid toluene. The spectrum is collected from a focal point within the bulk liquid,
28 away from the surface of the cover slip to avoid interference. The position of spectral peaks for toluene
29 is well characterized and these are used as a reference for wavelength calibration.

30 **2.3 Artificial Lung Chamber & Particle Imaging**

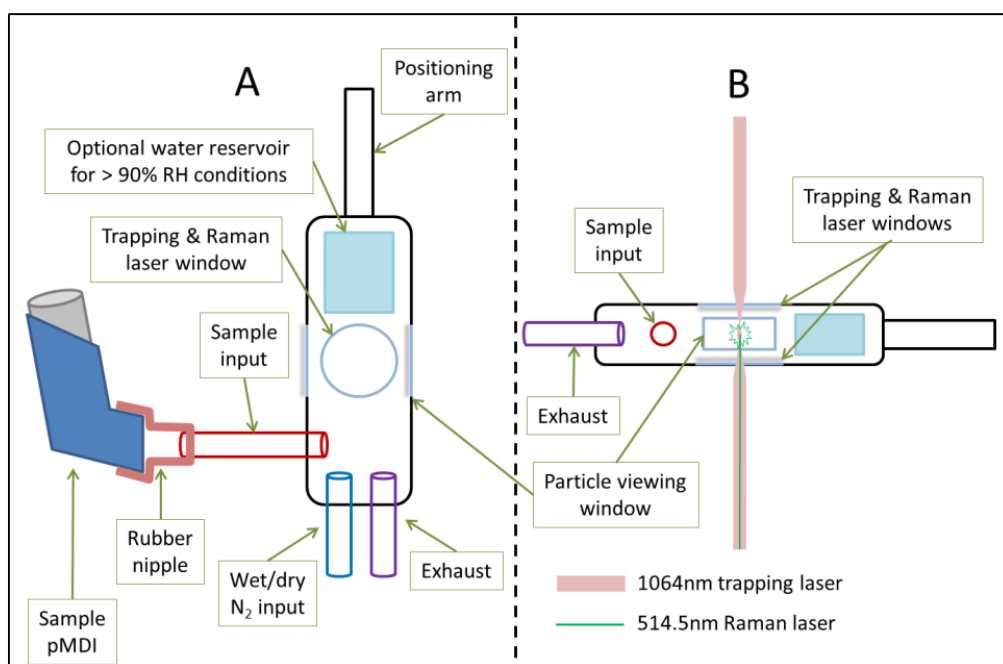


Figure 2 Top-down (A) and side (B) views of the artificial lung chamber
(High RH conditions here defined as >93% @ 20°C)

The artificial lung (figure 2) was an aluminium chamber of internal dimensions approximately 10 x 2 x 1cm, with borosilicate cover slip windows at the top and bottom to admit laser light and also at the sides to observe particles using a Mitutoyo M Plan Apo 20x objective lens connected to a CCD camera (Princeton Instruments, Spec10), opposite an LED source (Comar Optics). A monitor attached to the CCD camera allowed users to observe particles passing around, through and into the optical trap.

RH and temperature were monitored using a Sensirion SHT-75 RH probe with a manufacturer-stated accuracy of $\pm 1.8\%$ RH and $\pm 0.3^\circ\text{C}$. Raman spectra were collected within 3 minutes of reaching the desired RH. This is significantly longer than the 10 seconds recommended by the medical community for inhalation, holding an exhalation of a pMDI dose but is necessary for adjusting RH accurately and for developing clear and reproducible spectra. RH levels were altered using N_2 gas sourced from boiled off liquid nitrogen, using a flow rate of $\sim 200\text{ cm}^3/\text{min}$ through a Bronkhorst MV-301 mass flow controller. A lower flow rate of $100\text{ cm}^3/\text{min}$ was used for RH adjustment of the Salmeterol particles, since higher flow rates tended to dislodge the particles from the trap for reasons discussed in section 3.3. The input and exhaust ports were located on the same face of the cell in order to generate slow flow conditions around trapped particles and thus minimise turbulence that might dislodge the particle.

The gas was either run into the cell directly (low RH) or passed through a bubbler containing milli-Q grade deionized water before entering the cell (high RH). For very high RH conditions, a water reservoir was added inside the chamber. While the bubbler could provide RH up to $\sim 90\%$, the reservoir could generate RH as high as 93% at 30°C and up to 98% at 20°C .

Salmeterol xinafoate, fluticasone propionate and ciclesonide were analysed at ambient temperature at high and low RH. Salbutamol sulfate was analysed both at ambient temperature and at more

1 physiologically relevant temperatures by incubation of the microscope environment using Solent
2 Scientific incubator components.

3 **2.4 pMDI injection**

4 To dispense the aerosolised drug into the artificial lung chamber, a simple connector was built for the
5 pMDI outlet involving a flexible rubber cap with a rigid 6mm (internal diameter) PTFE tube protruding
6 through it. The tube was connected to a similar tube on the side of the artificial lung by a short length
7 of flexible silicone tubing. The chamber was washed sequentially in deionized water and methanol to
8 minimise potential cross-contamination with other drugs.

9 The propellant flow within the sample chamber carried material from each pMDI discharge into the
10 path of the trapping beam. Drug particles passing across the side viewing window were illuminated by
11 an LED and observed on a monitor. Scattering of the unfiltered trapping laser from a trapped particle
12 was viewed on the same monitor to indicate the positional stability of the particle.

13 Based on the stated mass per release of each drug, the density of the solid material (Zhejiang NetSun
14 Co., Ltd., 2010), the assumption that an average particle is solid and has a volume of approximately
15 $10\ \mu\text{m}^3$, a single release from each inhaler is estimated to deliver approximately 10^6 to 10^7 particles to
16 the chamber. However, many of these particles are lost by impaction onto the walls of the chamber.
17 A single trapped particle, which is at least $2\ \mu\text{m}$ in diameter, has sufficient material to generate a
18 Raman spectrum.

19 **2.5 SEM imaging**

20 Each drug was actuated onto a glass cover slip and coated with 10nm gold particles in a Polaron
21 SC7640 sputter coater. The cover slips were attached to Agar Scientific 25mm double sided sticky
22 carbon tabs prior to imaging on a Philips XL30 ESEM FEG.

23 **2.6 Chemical Structures of the asthma drugs investigated**

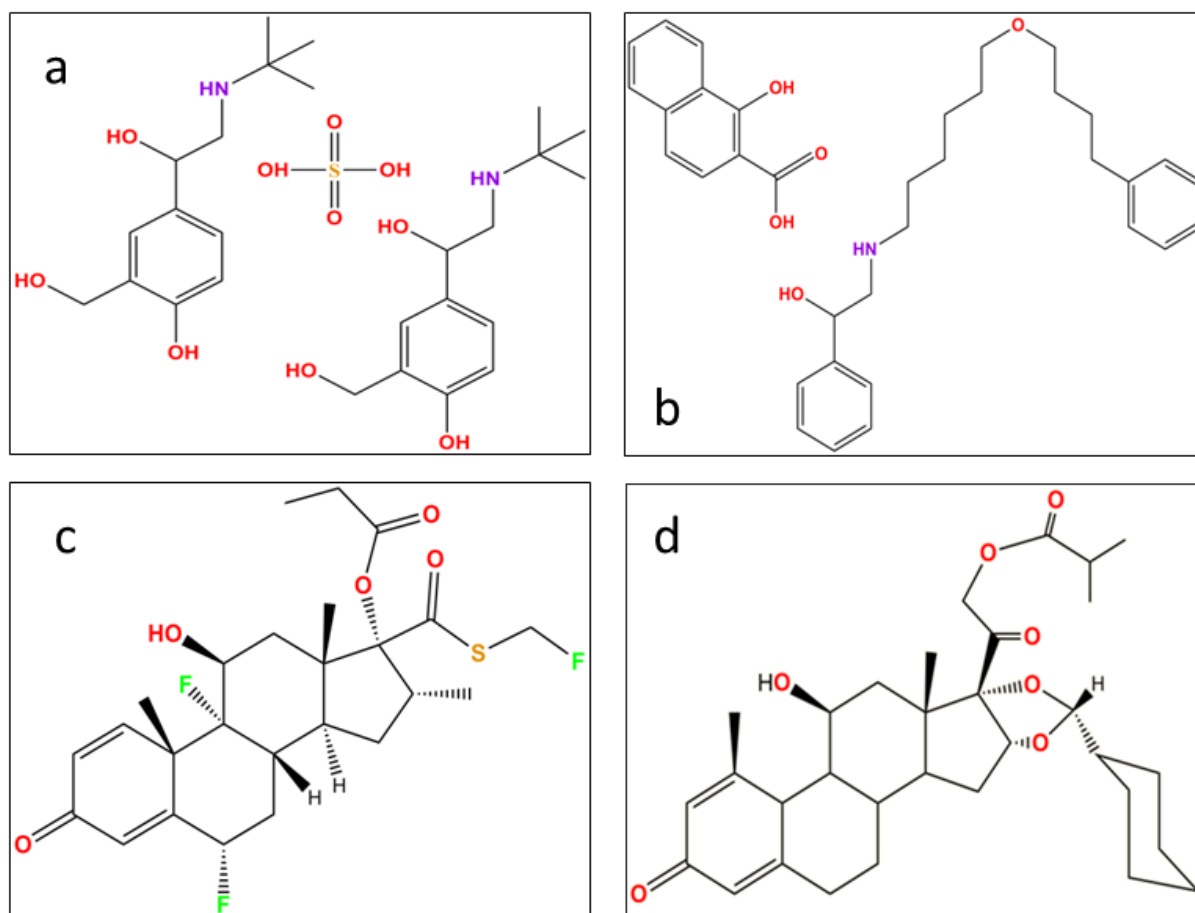


Figure 3 Chemical structures of single molecules of salbutamol sulfate (a), salmeterol xinafoate (b), fluticasone propionate (c), and ciclesonide (d)

Salbutamol sulfate particles were generated from a Salamol brand inhaler by Ivax Chemicals Ltd. Salbutamol sulfate contains several polar groups and no long aliphatic chains, and its hygroscopic character has been documented (Tong, et al., 2014). Salmeterol xinafoate particles were produced from a "Serevent" brand inhaler produced by Cipla Ltd. Salmeterol also contains multiple polar groups but also a long aliphatic chain. Its hygroscopic properties are to be determined.

Fluticasone propionate, generated from a "flixotide" brand inhaler, is manufactured by GlaxoSmithKline, and ciclesonide particles were generated by a "Ciclohale" brand inhaler also by Cipla Ltd. Ciclesonide is produced under license from Takeda UK Ltd. Fluticasone propionate and ciclesonide are both steroids and as such are relatively hydrophobic and are not expected to show hygroscopic properties.

3. Results and Discussion

3.1 Thermodynamic Calculations of Particle Hygroscopicity

Thermodynamic calculations of aerosol particle hygroscopicity were carried out using the Extended Aerosol Inorganics Model (E-AIM) (Clegg, et al., 2001) (Engelhart, et al., 2011) (Ling & Chan, 2008). E-AIM is a thermodynamic model for predicting the water content of aerosol particles at different RHs. The model is appropriate for calculating the thermodynamic state of the drug aerosol for a given RH, however, the model does not take into account the time dependent kinetic limitations of water uptake

1 to the particle within the respiratory tract. Within E-AIM, model III is used and the UNIFAC model is
 2 chosen to calculate the water activities of the organic fraction of the investigated drugs within the
 3 particle at different RH. The UNIFAC model parameterizes the molecular composition of the organic
 4 fractions of the investigated drug particle using a combination of structural and functional groups
 5 (Wittig, et al., 2003). The calculation of water activities of the sulfate group within salbutamol sulfate
 6 is also described by Clegg (Clegg & Brimblecombe, 1998). The type and quantity of UNIFAC parameters
 7 chosen to represent the four investigated drugs are provided in Table 1. It is noted in some cases
 8 exact matches for molecular composition, using UNIFAC, of the investigated drugs are not possible
 9 and in such cases the closest match was used. Standard dissociation constants for the carboxylic acid
 10 and amine functional groups were used. The model assumes that both salbutamol sulfate and
 11 salmeterol xinafoate dissociate into their respective ions dependent upon their dissociation constants.
 12 The formation of solid salts (salbutamol sulfate and salmeterol xinafoate) is disallowed since the
 13 activity products of the salts are unknown. Hence the modelled hygroscopicity provides an upper limit
 14 estimate.

15

16 Table 1. UNIFAC parameters used for thermodynamic modelling of the four investigated drugs. Note
 17 that the salmeterol xinafoate is modelled as two separate molecules: salmeterol and xinafoate. Also
 18 note that the sulphate in salbutamol sulphate is not modelled using UNIFAC hence its omission from
 19 the table.

UNIFAC Group	Salmeterol	Xinafoate	Salbutamol	Fluticasone propionate	Ciclesonide
Alkane (CH ₃)	-	-	3	4	3
Alkane (CH ₂)	10	-	1	1	9
Alkane (CH)	1	-	1	4	6
Alkene (CH=CH)	-	-	-	1	1
Alkene (CH=C)	-	-	-	1	1
Aromatic carbon (ACH)	8	6	3	-	-
Aromatic carbon (AC)	4	4	3	-	-
Alcohol (OH)	3	1	3	1	1
Carboxylic acid (COOH)	-	1	-	-	-
Carbonyl (CH ₂ CO)	-	-	-	2	2
Ether (CH ₂ O)	1	-	-	-	-
Ether (CHO)	-	-	-	-	2
Secondary amine (CH ₂ NH)	1	-	1	-	-

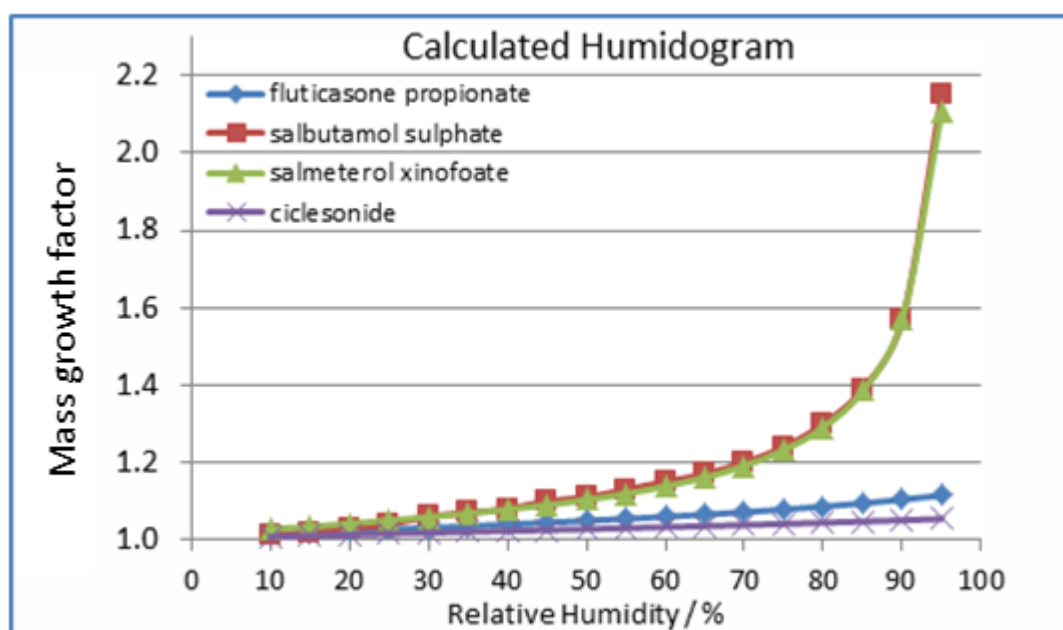
Acetate (CH ₂ COO)	-	-	-	1	1
Fluoroalkane (CF)	-	-	-	3	-

1

2

3 The output from E-AIM allows for the prediction of the drug molecule hygroscopicity (Clegg, et al.,
4 2001) (Engelhart, et al., 2011) (Ling & Chan, 2008). Figure 4 shows the mass growth factors for the
5 four investigated drugs. Mass growth factor is defined as the mass increase, for a given RH, normalized
6 to the dry mass. It can be seen that Figure 4 predicts two distinct types of interaction. The beta-2
7 agonists (salbutamol sulfate and salmeterol xinafoate) contain a higher proportion of hydrophilic
8 groups and are thus predicted to be strongly hygroscopic, while the more lipophilic steroids
9 (ciclesonide and fluticasone propionate) are expected to collect little water from the air even under
10 near water saturated conditions. It is noted, that the bulk thermodynamic calculations in E-AIM do
11 not take into account the crystal structure of solid particles which may block access to hydrophilic sites
12 and prevent otherwise hydrophilic molecules from interacting with water in the air. Furthermore, the
13 model runs do not take into account possible deliquescent barriers to water uptake due to the lack of
14 product activity data.

15 Ferron's kinetic model (Ferron, 1977), as used in the International Commission on Radiological
16 Protection (ICRP, 1994) provides a parameterization with which to estimate of the time dependent
17 growth of hygroscopic particles. pMDI particles are typically generated in the size range 2 – 5 μm to
18 optimally deliver drugs to the central regions of the lung. The Ferron model suggests that a
19 hygroscopic particle of initial size of 2–5 μm diameter will reach approximately 80–50% of its
20 equilibrium size, respectively, within a typical 2–3 s long inhalation.



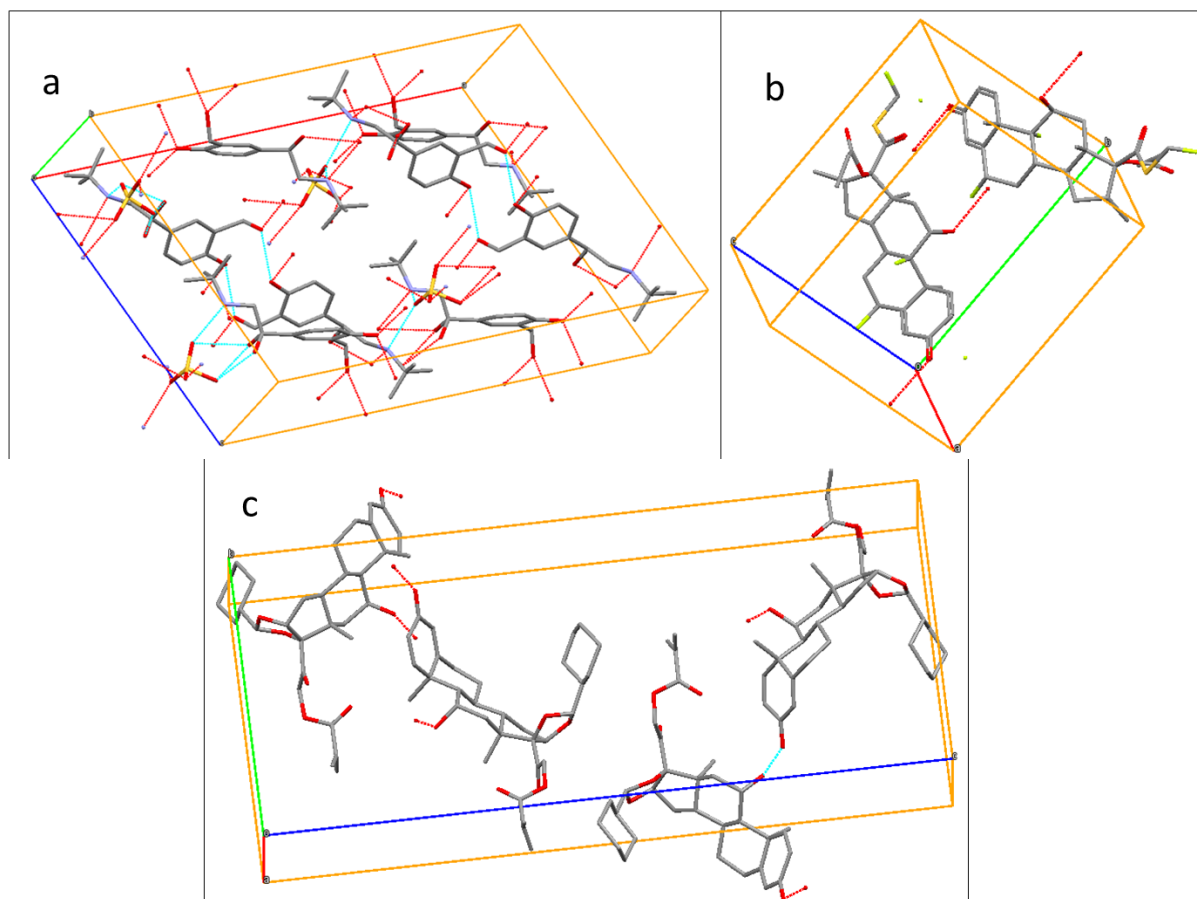
21

22

Figure 4 Influence of relative humidity on particle diameter predicted from chemical bonding

1 3.2 Drug Particle Crystallography

2 The Mercury 3.6 program (Macrae, et al., 2006) was used to simulate the crystal structure of all drugs
 3 whose structures had been added to the Cambridge Structural Database run by the Cambridge
 4 Crystallographic Data Centre (CCDC, 2015).



5
 6 Figure 5 Model unit cells of salbutamol sulfate (a), fluticasone propionate (b), and ciclesonide (c). Salmeterol xinafoate's
 7 unit cell was not available at time of writing. Hydrogen bonding within the unit cell is illustrated with a cyan line, while
 8 hydrogen bonding external to the unit cell (thus contributing to hygroscopic behaviour) are illustrated with red dotted
 9 lines.

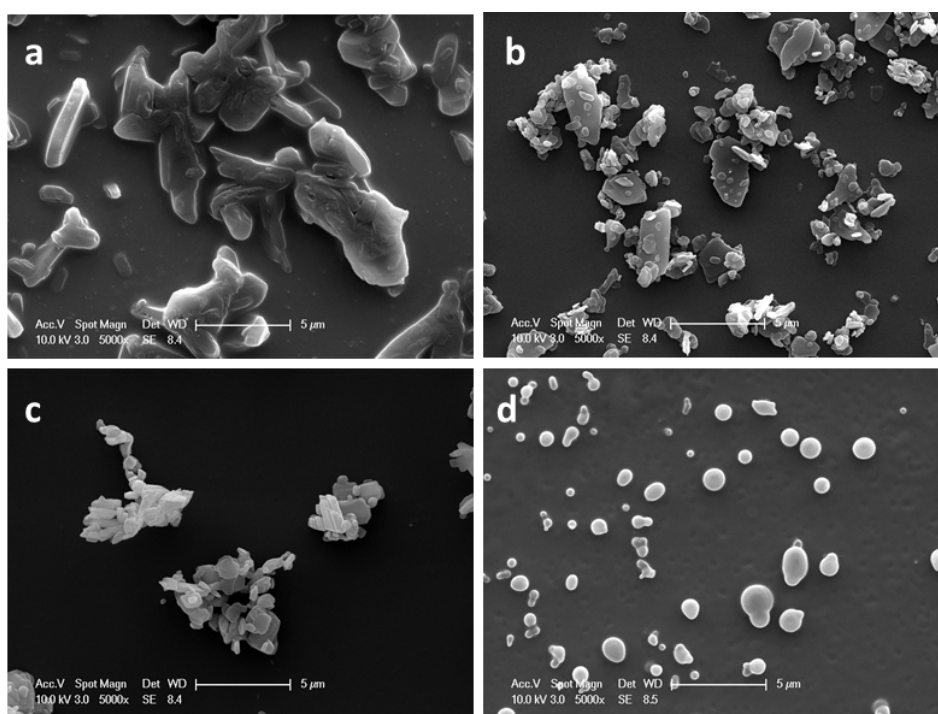
10 The chemical structure of salbutamol sulfate (figure 5a) shows hydrophilic sites across the molecule.
 11 The most likely crystal form generated by rapid solvent evaporation in air was first described in 1978
 12 (Leger, et al., 1978), with an 8 molecule unit cell (figure 5a) that shows hydrogen bonding sites on
 13 every face. Hygroscopic behaviour is inferred from this structure and has been demonstrated in
 14 previous experiments at room temperature (Tong, et al., 2014).

15 Salmeterol is not found in the Cambridge Structural Database. Solid structures are variously described
 16 as either amorphous, or needle-like or plate-like crystals depending on the exact conditions of
 17 manufacture (York & Hanna, 1994) (Barjoan & Clotet, 2009). Salmeterol xinafoate is bound together
 18 by hydrogen bonding of the δ -positive amine group on salmeterol to the δ -negative carboxylic acid
 19 group on the xinafoic acid. The two groups are expected to cancel their respective charges, leaving
 20 few hydrophilic sites open to interaction with water while the particle is in a solid state.

1 As a steroid, fluticasone is expected to be lipophilic (Lipworth & Jackson, 2000). The structure of
 2 fluticasone (figure 5b) does have a number of polar groups. However, the documented crystal
 3 structure (Cejka, et al., 2005) describes a plate-like structure with any hydrogen bonding occurring
 4 along the plane of growth (figure 5b) resulting in water interaction only along edges, and likely to
 5 result in little or no hygroscopic behaviour.

6 Ciclesonide (figure 5c) is found as either needle-like (Phull, et al., 2012) or needle-like and spherulitic
 7 crystals as well as amorphous solids (Feth, et al., 2007) depending on solvent type and evaporation
 8 time. Ciclesonide has multiple polar groups but the model unit cell described by Feth et al describes
 9 most of the oxygens arranged inside the crystal with the hydrophobic sites facing outward. Limited
 10 hydrogen bonding due to the hydroxyl and ketone groups on adjacent molecules have the potential
 11 to attract water molecules to crystal faces, but the hydrophobic nature of the rest of the exposed
 12 molecule implies that hygroscopic behaviour is unlikely.

13 3.3 SEM imaging and Trapping Logistics



14
 15 Figure 6 SEM images of: (a) salbutamol sulphate, (b) salmeterol xinafoate, (c) fluticasone propionate & (d) ciclesonide

16 SEM images of the drug particles were collected under dry conditions in order to determine shape and
 17 ease of capture. The likelihood of a particle being successfully caught in the optical trap is dictated by
 18 both particle shape and the number of particles generated per release. Salbutamol sulfate had been
 19 optically trapped previously on the same apparatus (Tong, et al., 2014). The thick, needle like shape
 20 of salbutamol sulfate particles (figure 6a) is well suited to entrapment for reasons detailed in section
 21 2.4, and the 100 µg per release dose of the available inhalers resulted in a successfully suspended
 22 particle roughly once for every two releases. Salmeterol xinafoate was significantly harder to trap and
 23 retain than the others due to a combination of its low dose (20 µg per release) and flat, platelike
 24 aggregate structure (figure 6b). Fluticasone has a similar crystal structure to salmeterol but a much
 25 higher dose (250 µg per release) and was more reliably trapped than salbutamol sulfate. Ciclesonide

1 was similar in trapping frequency to fluticasone since its lower dose (160 μg per release)
2 by a more spherical particle shape (figure 6d).

3 **3.4 Raman spectrum changes from hygroscopic properties and additional compounds**

4 Hydrogen bonding with water molecules adjacent to the polar groups of organic molecules expands
5 the range of vibrational energy states that can generate Raman scattering photons. This effect allows
6 water uptake by hygroscopic particles to be monitored by Raman spectroscopy.

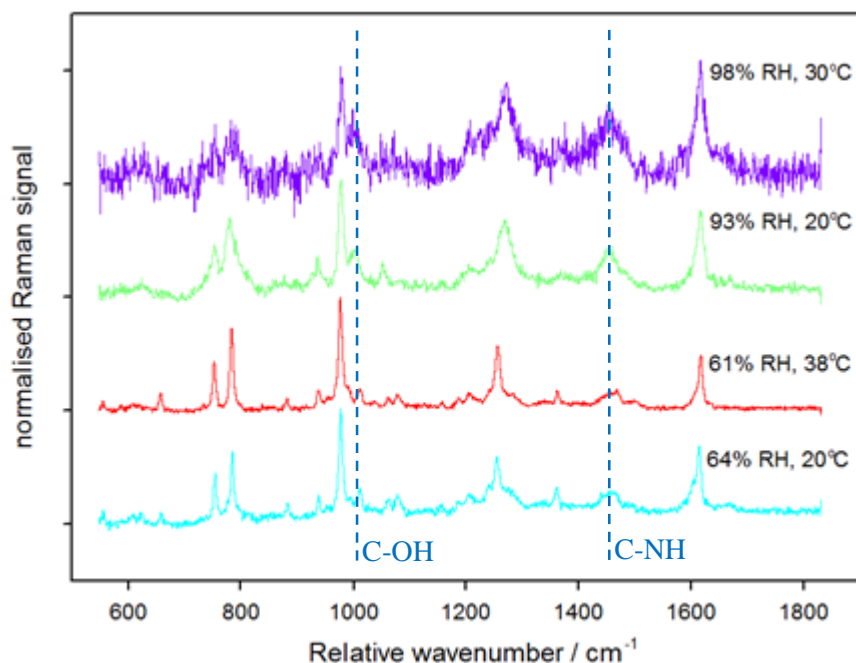
7 All four drugs use hydrofluoroalkane HFA 134a/Norflurane as a propellant. The salbutamol and
8 ciclesonide inhalers also report anhydrous ethanol among their ingredients. Norflurane contains four
9 C-F bonds, each of which generate a distinctive Raman scattering peak at 1234 cm^{-1} . This peak is not
10 expected to be visible in the Raman spectra of the drug molecules, apart from Fluticasone which has
11 3 C-F bonds of its own, due to Norflurane's low boiling point (-26.5°C , (Lide, 1991)) at atmospheric
12 pressure causing all of the propellant to boil off before readings can be collected. The spectra collected
13 from particles other than fluticasone do not show peaks in the C-F stretching region, which implies
14 that all propellant boils off before the particles are scanned.

15 **3.5 Salbutamol sulfate / Salamol™**

16 **3.5a Raman spectra and structural information**

17 Each salbutamol molecule contains a single phenol group, two aliphatic hydroxyls and a secondary
18 amine. One molecule of salbutamol contains two ionised salbutamol molecules bound to a single
19 sulfate group. The S=O symmetric stretches on the sulfate show a small but distinctive peak at 1154
20 cm^{-1} . The largest peaks in the salbutamol spectrum correspond to $-\text{CH}$ wagging at 656 cm^{-1} , aromatic
21 ring vibration at 752 cm^{-1} , C-C-O stretches in relation to the aliphatic hydroxyls at 784 cm^{-1} , asymmetric
22 hydroxyl stretches at $969, 977$ and 1008 cm^{-1} , phenyl ring vibrations at 1059 and 1074 cm^{-1} , a
23 prominent CH stretch at 1257 cm^{-1} (this bond can be found in figure 3 just above the ring) CH_2 and
24 CHOH vibrations again from the aliphatic hydroxyls at 1360 cm^{-1} , a broad ring stretching peak around
25 1450 cm^{-1} followed by a $\text{CH}_2\text{-N}$ amine peak at 1463 cm^{-1} , and finally a strong peak at 1615 cm^{-1}
26 corresponding to the phenolic C-OH stretch. All of these peaks (figure 7) correspond well with those
27 found in the literature (Ali, et al., 2009).

28 **3.5b Impact of RH and Temperature on salbutamol spectra**



1
 2 Figure 7 Raman spectra of optically trapped salbutamol sulfate particles at a range of RH and temperatures.
 3 Above salbutamol's deliquescence point of 92% RH, peak broadening is visible at the C–OH peak at 1008cm^{-1}
 4 and at the C–NH peak at 1463cm^{-1} , signifying water interaction with the bonds.

5 RH above 92%, the deliquescence point identified by Tong et al (Tong, et al., 2014), could not be
 6 maintained at physiological temperature (37°C) with the available equipment, so measurements were
 7 taken at 30°C - the highest temperature at which $>92\%$ RH could be maintained. The particle trapped
 8 at 98% RH and 30°C was small, hence the poorer signal/noise ratio. The contrast between the
 9 relatively dry and relatively wet particles is clear to see as the peaks corresponding to hydrophilic
 10 bonds in the wet particles are broader, and some peaks such as the hydroxyl peak at 1008cm^{-1} and
 11 the amine peak at 1463cm^{-1} are more pronounced.

12 The spectral traces, recorded at similar RH but under contrasting temperatures, are very similar.
 13 Within the temperature range investigated ($20\text{--}38^{\circ}\text{C}$), there are no observable temperature effects
 14 upon particle deliquescence. The deliquescence RH is measured to be ca. 92% RH in agreement with
 15 the measurement of Tong et al (Tong, et al., 2014). This implies that the temperature gradient
 16 experienced in the trajectory from pMDI to lung is likely to be unimportant in determining particle
 17 hygroscopicity; RH is the dominant determinant of particle hygroscopicity.

18 The modelling results from E-AIM suggested that salbutamol sulfate would show significant
 19 hygroscopicity if a deliquescence phase transition occurred. The experimental results confirm this
 20 model prediction. The presence of a phase transition and significant water uptake is in line with the
 21 high reported solubility of salbutamol sulfate (14.1g/L , (Walkowsky & He, 2003).

22 3.6 Salmeterol xinafoate / Serevent™

23 3.6a Raman spectra and structural information

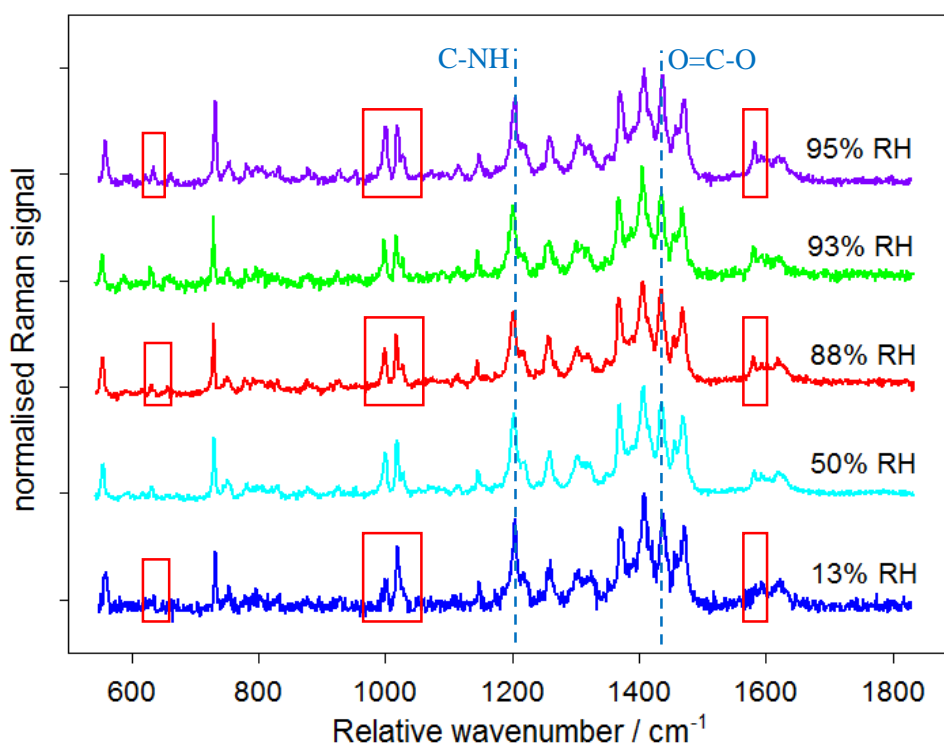
24 Salmeterol xinafoate contains several aromatic rings, an ether group, a benzoic acid and a secondary
 25 amine. Benzoic acid is distinct from both aromatic rings and carboxylic acids due to the increased

1 conjugation (Kwon, et al., 1994) and shows distinctive peaks in the solid state at 1627 cm^{-1} , 994 cm^{-1}
 2 and 788 cm^{-1} . These peaks are all present in our spectra (figure 8). Ring stretches are clearly visible at
 3 $1580\text{-}1616\text{ cm}^{-1}$, $1400\text{-}1420\text{ cm}^{-1}$ (the multiple strong peaks denoting ring stretches shifted by the
 4 various adjacent functional groups) and symmetric ring stretches are visible at $1000\text{-}1028\text{ cm}^{-1}$, 1215
 5 and 1257 cm^{-1} . A strong amine vibration peak is visible at 1204 cm^{-1} . A sharp peak at 730 cm^{-1}
 6 corresponds to rotational peaks from CH_2 groups, as would be expected by a molecule with a long
 7 aliphatic chain like salmeterol. The ether group can be identified by small peaks at 554 and 1145 cm^{-1} .
 8 These spectra correspond well with previously published, well-defined Raman spectra (Ali, et al.,
 9 2008a).

10 Repeated exposure to the Raman laser caused some fluorescence effects in salmeterol xinafoate
 11 particles, so each spectrum had to be recorded on a freshly captured particle. The Raman laser was
 12 blocked except during the collection of spectra in order to minimise the effect. The fluorescence
 13 activity that occurs in salmeterol xinafoate after prolonged exposure to the Raman laser may possibly
 14 be avoided in future experiments by using a longer excitation wavelength.

15

16 3.5b Impact of RH on salmeterol spectra



17

18 Figure 8 Raman spectra of salmeterol xinafoate at a range of RH values. Even at 95% RH, the amine vibrational
 19 peak at 1204 cm^{-1} and carboxylic acid stretching peak at 1420 cm^{-1} do not show signs of broadening, contrary to
 20 the predicted behaviour modelled by E-AIM. Intensity changes on the aromatic ring stretches at different RH are
 21 highlighted in red.

22 According to the Raman spectra collected in figure 8, salmeterol xinafoate does not demonstrate any
 23 visible broadening around peaks corresponding to either salmeterol's amine group or the carboxylic
 24 acid group on its xinafoic acid partner upon RH enhancement. This suggests that the salt does not
 25 undergo a deliquescent phase transition. The modelling results from E-AIM suggested that salmeterol

1 xinafoate would show significant hygroscopicity if a deliquescence phase transition occurred. The
2 observed lack of deliquescence is in line with the low predicted solubility of salmeterol xinafoate (22.6
3 mg/L according to ALOGPS (Tetko, 2001)).

4 The hygroscopic behaviour of salmeterol xinafoate, as predicted by E-AIM, may be limited by the steric
5 hindrance of the hydrophilic sites by hydrophobic structures arranged around them in solid crystals.
6 The relative enhancement of peaks corresponding to aromatic ring stretches at 650, 1000 and 1580
7 cm^{-1} imply some interaction with water around some or all of the aromatic rings in salmeterol
8 xinafoate at >88% RH. Most likely, the presence of the hydroxyl and carboxylate groups on the
9 aromatic xinafoate section of the drug enhances water interaction.

10 **3.4 Fluticasone propionate / Flixotide**

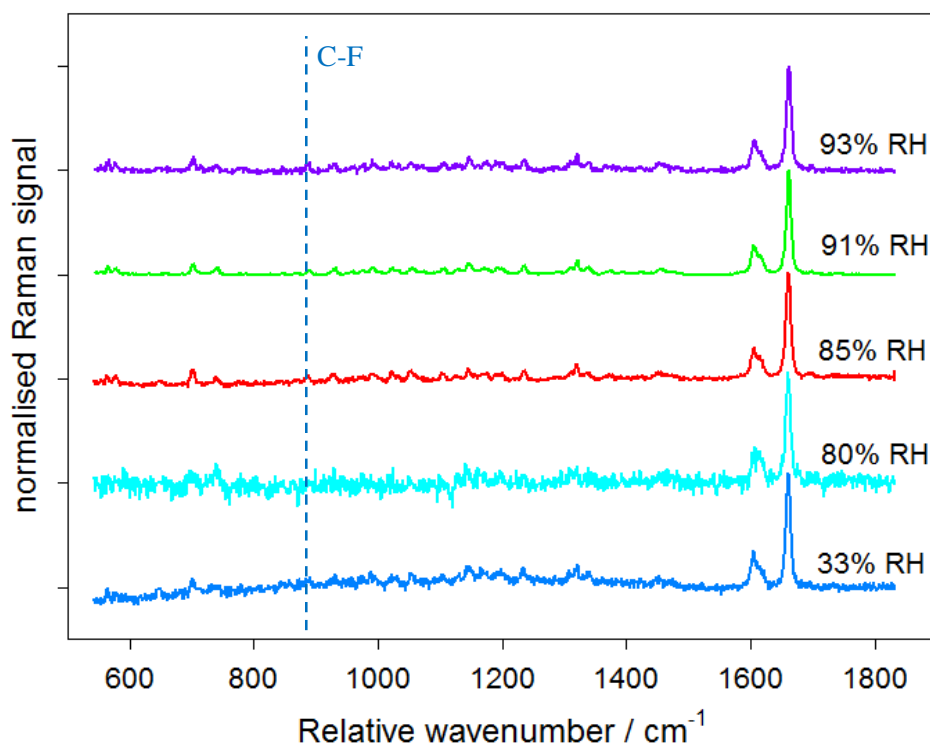
11 **3.4a Raman spectra and structural information**

12 Fluticasone contains several distinctive bonding types that would be expected to yield distinctive
13 peaks in any resulting Raman spectra: a phenone, an ester, a thioether and three C-F bonds across the
14 molecule. Fluticasone has been imaged by Raman spectroscopy previously and its spectra interpreted
15 in depth (Ali, et al., 2008b) (Rogueda, et al., 2011) (Theophilus, et al., 2006) (Wang, et al., 2014), which
16 provides useful references for the spectra generated here.

17 The raw fluticasone propionate spectra contained a very sharp and strong peak at 640 - 650 cm^{-1} . This
18 peak was not observed in other spectra in the literature. We believe this peak to be an artefact caused
19 by second harmonic resonance effect from the 1064 nm trapping laser. Confirmation of the spectral
20 artefact was achieved by measuring spectra of fluticasone propionate recorded on the cover slip
21 without the trapping laser present. These spectra did not contain the peak. We have removed this
22 artificial peak from the spectra shown in Figure 9.

23 The strongest peak in the spectrum of fluticasone is the C=O vibration at 1659 cm^{-1} , followed by the –
24 CH_3 symmetric stretch (there are 4 – CH_3 groups in Fluticasone) at 1606 cm^{-1} . – CH_2 and –CH stretches
25 occur at around 1380 and 1330 cm^{-1} respectively and highly distinctive C-F and S-C-F bands occur at
26 1234 cm^{-1} and 1022 cm^{-1} . Fluticasone is the only compound among the samples that contains a C-F
27 bond, and generated the only spectra showing C-F stretching peaks. This implies that that in all
28 samples the Norflurane propellant had fully evaporated prior to analysis. The phenone group registers
29 as an OOH/CCH aromatic deformation peak at 888 cm^{-1} . A small C-H wagging peak can be seen at
30 around 700 cm^{-1} .

31 **3.4b Impact of RH on fluticasone spectra**



1
 2 Figure 9 Raman spectra of fluticasone propionate at a range of RH values. The C-F stretching peak at 888 cm^{-1}
 3 is present in this spectrum but not the others, confirming that the Norflurane propellant discussed in section 3.4
 4 has boiled off

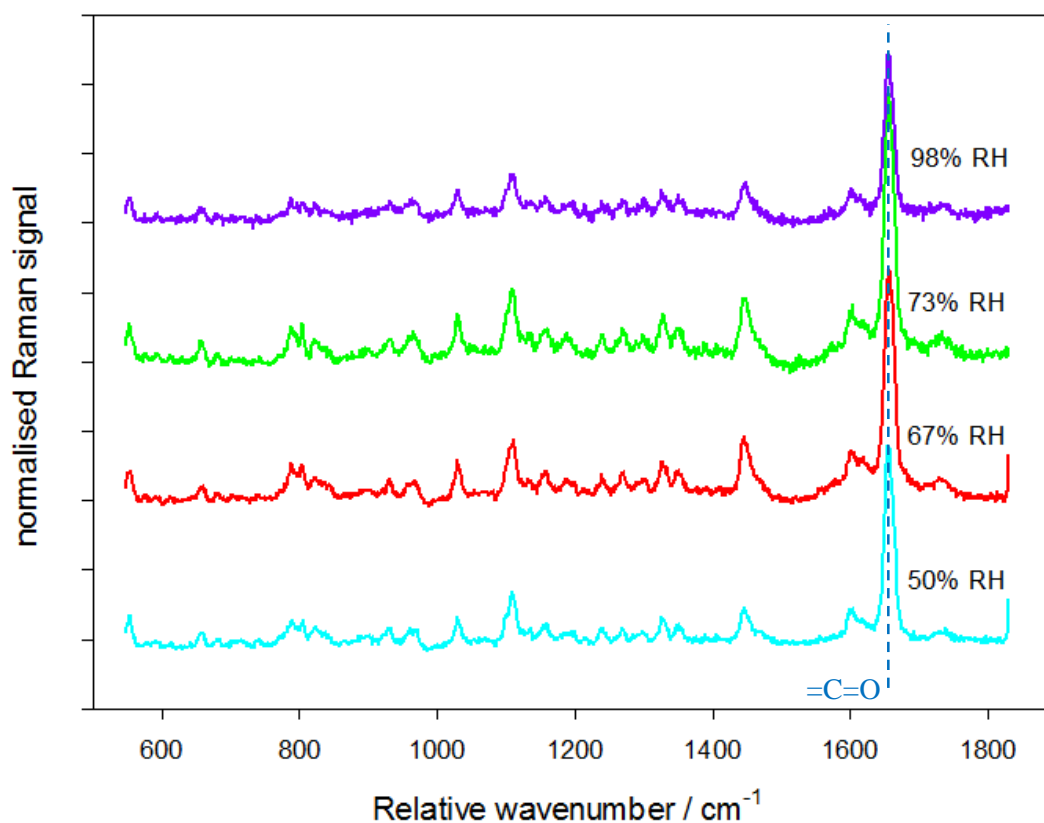
5 The spectrum collected at 80% RH was from a small particle- around $1\mu\text{m}$ in diameter. This accounts
 6 for the greater noise in the signals. Otherwise, no peaks are displaced or strongly deformed by the rise
 7 in relative humidity. Fluticasone shows no signs of hygroscopic behaviour, in agreement with the
 8 results from E-AIM. Water solubility is low (11.4 mg/L) as predicted by ALOGPS (Tetko, 2001).

9 3.5 Ciclesonide / Alvesco™

10 3.5a Raman spectra and structural information

11 Ciclesonide (Feth, et al., 2008) has a diverse selection of functional groups, which generates a
 12 complicated Raman spectrum. The largest peak at 1654 cm^{-1} (figure 10) represents the stretching
 13 vibration of an α , β -unsaturated carbonyl, while the adjacent peak at 1601 cm^{-1} shows the
 14 neighbouring C=C bond. Ciclesonide contains four $-\text{CH}_3$ groups and this corresponds to another large,
 15 broad peak at 1443 cm^{-1} . The three ether bonds generate another large peak at 1112 cm^{-1} , and the
 16 single ester linkage appears at 1242 cm^{-1} . Ciclesonide has a single hydroxyl group attached to a six-
 17 membered saturated ring, and a matching "cyclic alcohol" stretch appears at 1029 cm^{-1} . The C-C
 18 stretches of the two saturated six-membered rings are found at 963 cm^{-1} . Multiple small peaks around
 19 $800\text{-}900\text{ cm}^{-1}$ represent ring deformation in the phenol group adjacent to the saturated rings. Another
 20 region of small peaks around 1330 cm^{-1} corresponds to the various symmetric and antisymmetric
 21 stretches of the isopropyl group.

22 3.5b Impact of RH and Temperature on Ciclesonide Spectra



1

2 Figure 10 Raman spectra of ciclesonide at a range of RH values. The spectra show no signs of hygroscopic
 3 behaviour at up to 98% RH.

4 As a steroid, ciclesonide is not very hydrophilic and does not contain many polar groups. The crystal
 5 structure shows very little opportunity for water uptake on surfaces, and E-AIM predicts that
 6 ciclesonide has the lowest hygroscopic potential of any of the drugs analysed. Calculated water
 7 solubility is also the lowest of all the drugs (1.57mg/L, (Tetko, 2001)). It would not be expected to show
 8 hygroscopic behaviour, and no such behaviour was observed in the Raman spectra compiled in figure
 9 10.

10

11 3.6 Specific advantages and limitations of procedure to drug delivery

12 The advantages of this setup and analytical technique to the examination of inhalable drugs do merit
 13 some discussion in addition to the general benefits of optical trapping over cover slip analysis
 14 documented in section 2.1. The current setup can monitor particle size with an external camera as
 15 well as directly monitoring water interactions with hydrophilic functional groups on particles by
 16 examining the Raman spectrum. On-board RH monitoring can determine deliquescence points for new
 17 drugs, or verify those of existing drugs, to a high degree of accuracy, factoring in the crystal structures
 18 of particles as well as their chemical structure in a manner that is difficult to reproduce with software
 19 modelling alone. At present, the main limitation of the technique is the length of time required to
 20 collect each Raman spectrum which is longer than the pMDI inhalation cycle.

21

22 4. Conclusions

1 This series of experiments has demonstrated a viable technique for examining individual particles of
2 inhalable drugs supplied by pMDIs. With little modification, such as by attaching a vacuum pump to
3 the outlet port of the sample chamber, this experimental setup may also be used to examine single
4 particles from DPI devices.

5 The Raman spectra of four optically trapped drug particles (salbutamol sulfate, salmeterol xinafoate,
6 fluticasone propionate and ciclesonide) were measured within a model lung. The model lung allowed
7 for modification of local RH to test the drugs for hygroscopic behaviour, while the optical trap
8 eliminated any surface effects from water droplets forming around a solid particle on a cover slip.
9 Raman spectroscopy allowed for the direct observation of the hydrogen bonding with water in
10 hydrophilic groups, where the broadening of peaks indicates hygroscopicity.

11 Spectral peak broadening was observed in salbutamol sulfate particles above their deliquescence
12 point at 92% RH, at room temperature and more physiologically relevant temperatures, while spectra
13 remained similar to dry particles at lower RH regardless of temperature within the observed range.
14 Salmeterol xinafoate shows some spectral changes to the intensities of the peaks corresponding to its
15 aromatic rings, but does not show any changes to the more hydrophilic functional groups which is
16 interpreted as no deliquescence at RH up to 95%. Fluticasone propionate and ciclesonide show no
17 hygroscopic properties at all, as would be expected with their lipophilic composition, low water
18 solubility and the modelled particle growth factors generated using the E-AIM model.

19

20 **Acknowledgements**

21 MKK is thankful to the EPSRC for the Career Acceleration Fellowship (EP/I003983/1). ND thanks
22 NERC for a personal studentship. MK was supported by ERC grant 279405. We are thankful to the
23 STFC for a programmed access grant LSF1207 (FLIMOLA).

24 **Works Cited**

25 Ali, Edwards, Kendrick & Scowen, 2008b. Vibrational spectroscopic study of fluticasone propionate.
26 *Biomolecular Spectroscopy*, pp. 244-247.

27 Ali, Edwards, Kendrick & Scowen, 2009. Vibrational spectroscopic study of salbutamol
28 hemisulphate. *Drug Testing and Analysis*, pp. 51-56.

29 Ali, et al., 2008a. Vibrational spectroscopic characterisation of salmeterol xinafoate polymorphs and a
30 preliminary investigation of their transformation using simultaneous in situ portable Raman
31 spectroscopy and differential scanning calorimetry. *Analytica Chimica Acta*, pp. 103-112.

32 Ashkin, 1992. Forces of a single-beam gradient laser trap on a dielectric sphere in the ray optics
33 regime. *Biophysical Journal*, pp. 569-582.

34 Barjoan & Clotet, 2009. Spain, Patent No. EP2127641A1.

- 1 Bell & Newman, 2007. The rejuvenated pressurised metered dose inhaler. *Expert Opinion on Drug*
2 *Delivery*, pp. 215-234.
- 3 Bikiaris, 2011. Solid dispersions, Part I: recent evolutions and future opportunities in manufacturing
4 methods for dissolution rate enhancement of poorly water-soluble drugs. *Expert Opinion on Drug*
5 *Delivery*, pp. 1501-1519.
- 6 Bloxham, Eicher-Lorka, J. & Niaura, 2002. The C-S bond in ethylthiols: a study of the characteristic
7 Raman vibrational Spectral Band. *Chemija*, 13(4), pp. 190-193.
- 8 Brain, Kreyling & Godleski, 2014. Inhalation Toxicology. In: Wallace & Kruger, eds. *Hayes'*
9 *Principles and Methods of Toxicology, Sixth Edition*. Boca Raton, FL: CRC Press, pp. 1402-1414.
- 10 Broday & Georgopoulos, 2001. Growth and Deposition of Hygroscopic Particulate Matter in the
11 Human Lungs. *Aerosol Science and Technology*, p. 144-159.
- 12 Bur, Huwer, Muys & Lehr, 2010. Drug Transport Across Pulmonary Epithelial Cell Monolayers:
13 Effects of Particle Size, Apical Liquid Volume, and Deposition Technique. *Journal of Aerosol*
14 *Medicine and Pulmonary Drug Delivery*, 3(23), pp. 119-127.
- 15 Calverley, et al., 2003. Combined salmeterol and fluticasone in the treatment of chronic obstructive
16 pulmonary disease: a randomised controlled trial. *The Lancet*, pp. 449-456.
- 17 CCDC, 2015. *WebCSD v1.1.1*. [Online]
18 Available at: <http://webcsd.cds.rsc.org/index.php>
19 [Accessed 10 11 2015].
- 20 Cejka, Kratochvil & Jegorov, 2005. Crystal Structure of Fluticasone Propionate, C₂₅H₃₁F₃O₅S.
21 *Zeitschrift für Kristallographie - New Crystal Structures*, pp. 143-144.
- 22 Chapman, et al., 1999. Salmeterol and fluticasone propionate (50/250 microg) administered via
23 combination Diskus inhaler: as effective as when given via separate Diskus inhalers.. *Canadian*
24 *Respiratory Journal: Journal of the Canadian Thoracic Society*, pp. 45-51.
- 25 Clark, 1994. Medical Aerosol Inhalers: Past, Present, and Future. *Aerosol Science & Technology*, pp.
26 374-391.
- 27 Clegg & Brimblecombe, 1998. A thermodynamic model of the system H⁺ - NH₄⁺ - Na⁺ - SO₄²⁻ -
28 NO₃⁻ - Cl⁻ - H₂O at 298.15 K. *The Journal of Physical Chemistry*, 12(102), pp. 2155 - 2171.
- 29 Clegg, Seinfeld & Brimblecombe, 2001. Thermodynamic modelling of aqueous aerosols containing
30 electrolytes and dissolved organic compounds. *Journal of Aerosol Science*, Issue 32, pp. 713-738.
- 31 Coates, 2000. Interpretation of Infrared Spectra, A Practical Approach. In: *Encyclopedia of Analytical*
32 *Chemistry*. Chichester: John Wiley & Sons Ltd, pp. 10815-10837.
- 33 Cripps, Riebe, Schulze & Woodhouse, 2000. Pharmaceutical transition to non-CFC pressurized
34 metered dose inhalers. *Respiratory Medicine*, 94(2), pp. S3-S9.
- 35 Crosland, Johnson & Matida, 2009. Characterization of the spray velocities from a pressurized
36 metered-dose inhaler. *Journal of Aerosol Medicine and Pulmonary Drug Delivery*, pp. 85-97.

- 1 Delgado, Chou, Silver & Crain, 2003. Nebulizers vs metered-dose inhalers with spacers for
2 bronchodilator therapy to treat wheezing in children aged 2 to 24 months in a pediatric emergency
3 department.. *Archives of Pediatric and Adolescent Medicine*, pp. 76-80.
- 4 Dodson, et al., 2011. Photophysical and photochemical properties of the pharmaceutical compound
5 salbutamol in aqueous solutions. *Chemosphere*, pp. 1513-1523.
- 6 Dolovich, Ruffin, Roberts & Newhouse, 1981. Optimal delivery of aerosols from metered dose
7 inhalers. *Chest*, 80(6), pp. 911-915.
- 8 Engelhart, et al., 2011. Water content of aged aerosol. *Atmospheric Chemistry & Physics*, Issue 11,
9 pp. 911-920.
- 10 Eom, et al., 2014. Influence of collecting substrates on the characterization of hygroscopic properties
11 of inorganic aerosol particles.. *Analytical Chemistry*, 4(86), pp. 2648-2656.
- 12 Ferron, 1977. The size of soluble aerosol particles as a function of the humidity of the air. Application
13 to the human respiratory tract. *Journal of Aerosol Science*, Volume 8, pp. 251-277.
- 14 Feth, et al., 2008. USA, Patent No. US20100120737 A1.
- 15 Feth, et al., 2007. Physicochemical, Crystallographic, Thermal, and Spectroscopic Behavior of
16 Crystalline and X-ray Amorphous Ciclesonide. *Pharmaceutics, Preformulation and Drug Delivery*,
17 pp. 3765-3780.
- 18 Haddrell, et al., 2014. Dynamics of aerosol size during inhalation: Hygroscopic growth of commercial
19 nebulizer formulations. *International Journal of Pharmaceutics*, pp. 50-61.
- 20 Harding, 1990. The human pharmacology of fluticasone propionate. *Respiratory Medicine*, pp. 25-29.
- 21 Hardy & Chadwick, 2000. Sustained Release Drug Delivery to the Lungs. *Clinical Pharmacokinetics*,
22 pp. 1-4.
- 23 Hargreaves, et al., 2010. Measurements of the Equilibrium Size of Supersaturated Aqueous Sodium
24 Chloride Droplets at Low Relative Humidity Using Aerosol Optical Tweezers and an Electrodynamic
25 Balance. *The Journal of Physical Chemistry*, pp. 1806-1815.
- 26 Hirschfeld & Chase, 1986. FT-Raman Spectroscopy: Development and Justification. *Applied*
27 *Spectroscopy*, 08 January, pp. 133-137.
- 28 Huang, et al., 2003. Near-infrared Raman spectroscopy for optical diagnosis of lung cancer.
29 *International Journal of Cancer*, pp. 1047-1052.
- 30 Hung, Chu, Wang & Yang, 1999. Hypoalkaemia and salbutamol therapy in asthma. *Pediatric*
31 *Pulmonology*, pp. 27-31.
- 32 Hunt, Ward & King, 2013. Laser heating of sulfuric acid droplets held in air by Raman tweezers. *RSC*
33 *Advances*, pp. 19448-19454.
- 34 Hunt, Ward & King, 2015. Heterogeneous oxidation of nitrite anion by gas phase ozone in an aqueous
35 droplet levitated by laser tweezers (optical trap): is there any evidence for enhanced surface reaction?.
36 *Physical Chemistry Chemical Physics*, pp. 2734-2741.

- 1 Ibrahim, Verma & Garcia-Contreras, 2015. Inhalation drug delivery devices: technology update.
2 *Medical Devices (Auckland)*, Volume 8, pp. 131-139.
- 3 Icha, 2007. Ventolin remains a breath of fresh air for asthma sufferers, after 40 years. *The*
4 *Pharmaceutical Journal*, p. 404.
- 5 ICRP, 1994. *Ann. ICRP 24 (1-3) publication 66: Human Respiratory Tract Model for Radiological*
6 *Protection*, s.l.: Elsevier Health Sciences.
- 7 Janson, et al., 2016. Difference in resistance to humidity between commonly used dry powder
8 inhalers: an in vitro study. *npj Primary Care Respiratory Medicine*, Issue 23, p. 16053.
- 9 Jones, King & Ward, 2015. Atmospherically relevant core-shell aerosol studied using optical trapping
10 and Mie scattering. *Chemical Communications*, pp. 4914-4917.
- 11 Kwon, et al., 1994. Vibrational Spectroscopic Investigation of Benzoic Acid Adsorbed on Silver.
12 *Journal of Physical Chemistry*, pp. 8481-8487.
- 13 Labiris & Dolovich, 2003. Pulmonary drug delivery. Part I: Physiological factors affecting therapeutic
14 effectiveness of aerosolized medications. *Journal of Clinical Pharmacology*, p. 588-599.
- 15 Lavorini, et al., 2011. Retail sales of inhalation devices in European countries: So much for a global
16 policy. *Respiratory Medicine*, pp. 1099-1103.
- 17 Lawrence, 2005. The relationship between relative humidity and the dew point temperature in moist
18 air: A simple conversion and applications. *Bulletin of the American Meteorological Society*, pp. 225-
19 233.
- 20 Leach, 2005. The CFC to HFA Transition and Its Impact on Pulmonary Drug Development.
21 *Respiratory Care*, 50(9), pp. 1201-1208.
- 22 Lee, et al., 2012. The Efficacy of Immediate Diet for Reducing Local Adverse Events of Inhaled
23 Corticosteroid: A Pilot Study. *Tuberculosis and Respiratory Diseases*, pp. 93-99.
- 24 Leger, Goursolle & Gadret, 1978. Structure Cristalline du Sulfate de Salbutamol [tert-Butylamino-2
25 (Hydroxy-4 hydromethyl-3 phenyl)-1 Ethanol.1/2H₂SO₄]. *Acta Crystallographica Section B*, pp.
26 1203-1208.
- 27 Lide, 1991. *CRC Handbook of Chemistry and Physics*. Boca Raton, FL: CRC Press.
- 28 Ling & Chan, 2008. Partial crystallization and deliquescence of particles containing ammonium
29 sulfate and dicarboxylic acids. *Journal of Geophysical Research*, 113(14), pp. 1-15.
- 30 Lipasek, et al., 2013. Effect of Temperature on the Deliquescence Properties of Food Ingredients and
31 Blends. *Journal of Agricultural and Food Chemistry*, pp. 9241-9250.
- 32 Lipworth & Jackson, 2000. Safety of Inhaled & Intranasal Corticosteroids Lessons for the New
33 Millennium. *Drug Safety*, 1(23), pp. 11-33.
- 34 Macrae, et al., 2006. Mercury: visualization and analysis of crystal structures. *Journal of Applied*
35 *Crystallography*, Volume 39, pp. 453-457.
- 36 Mansour, et al., 2016. 11.4 Particle deposition in the airways. In: Hillary & Park, eds. *Drug Delivery:*
37 *Fundamentals and Applications, Second Edition*. Boca Raton, FL: CRC Press.

- 1 Mutch, et al., 2007. The role of esterases in the metabolism of ciclesonide to desisobutyryl-
2 ciclesonide in human tissue. *Biochemical Pharmacology*, pp. 1657-1664.
- 3 Nave, 2004. *Saturated Vapor Pressure, Density for Water*. [Online]
4 Available at: <http://hyperphysics.phy-astr.gsu.edu/HBASE/Kinetic/watvap.html#c1>
5 [Accessed 6th August 2014].
- 6 Newman, N., 1996. Effect of add-on devices for aerosol drug delivery: Deposition studies and clinical
7 aspects. *Journal of Aerosol Medicine: Deposition, clearance and effects in the lung*, 9(1), pp. 55-70.
- 8 Newman, et al., 1981. Deposition of pressurised aerosols in the human respiratory tract. *Thorax*,
9 Volume 36, pp. 52-55.
- 10 Pandya, Berawala, Khatri & Mehta, 2010. Spectrofluorimetric estimation of salbutamol sulphate in
11 different dosage forms by formation of inclusion complex with β -cyclodextrin. *Pharmaceutical*
12 *Methods*, pp. 49-53.
- 13 PerkinElmer Inc, 2008. *Advantages of Raman Spectroscopy when Analysing Materials through Glass*
14 *or Polymer Containers and in Aqueous Solution*. [Online]
15 Available at:
16 [http://www.perkinelmer.co.uk/CMSResources/Images/APP_RamanAnalysisThrougGlassPolymerAq](http://www.perkinelmer.co.uk/CMSResources/Images/APP_RamanAnalysisThrougGlassPolymerAqueous.pdf)
17 [ueous.pdf](http://www.perkinelmer.co.uk/CMSResources/Images/APP_RamanAnalysisThrougGlassPolymerAqueous.pdf)
18 [Accessed 07 August 2014].
- 19 Phull, Rao & Kankan, 2012. United States of America, Patent No. US 8158780 B2.
- 20 Purewal & Grant, 1997. *Metered Dose Inhaler Technology (Illustrated ed.)*. s.l.:Informa Health Care.
- 21 Reisine, Heisler, Hook & Axelrod, 1983. Activation of beta 2-adrenergic receptors on mouse anterior
22 pituitary tumor cells increases cyclic adenosine 3':5'-monophosphate synthesis and
23 adrenocorticotropin release. *The Journal of Neuroscience*, pp. 725-732.
- 24 Renner, Mueller & Shephard, 2012. Environmental and non-infectious factors in the aetiology of
25 pharyngitis (sore throat). *Inflammation Research*, pp. 1041-1052.
- 26 Rkiouak, et al., 2014. Optical trapping and Raman spectroscopy of solid particles. *Physical Chemistry*
27 *Chemical Physics*, pp. 11426-11434.
- 28 Rogueda, et al., 2011. Particle synergy and aerosol performance in non-aqueous liquid of two
29 combinations metered dose inhalation formulations: An AFM and Raman investigation. *Journal of*
30 *Colloid and Interface Science*, pp. 649-655.
- 31 Sanders, 2007. Inhalation therapy: an historical review. *Primary Care Respiratory Journal*, pp. 71-81.
- 32 Sauer, Hofkens & Enderlein, 2011. *Handbook of Fluorescence Spectroscopy and Imaging*. Weinheim:
33 WILEY-VCH Verlag GmbH.
- 34 Stein, M., 2006. The Relative Influence of Atomization and Evaporation on Metered Dose Inhaler
35 Drug Delivery Efficiency. *Aerosol Science and Technology*, Issue 40, pp. 335-347.
- 36 Tang, et al., 2014. Heterogeneous interaction of SiO₂ with N₂O₅: single particle optical levitation-
37 Raman spectroscopy and aerosol flow tube studies. *The Journal of Physical Chemistry*, pp. 8817-
38 8827.

- 1 Tetko, 2001. *ALOGPS*. [Online]
2 Available at: <http://www.vcclab.org/lab/alogps/>
3 [Accessed 21 10 2016].
- 4 Theophilus, et al., 2006. Co-deposition of salmeterol and fluticasone propionate by a combination
5 inhaler. *International Journal of Pharmaceuticals*, pp. 14-22.
- 6 Tong, et al., 2014. Rapid interrogation of the physical and chemical characteristics of salbutamol
7 sulphate aerosol from a pressurised metered-dose inhaler (pMDI). *Chemical Communications*, pp.
8 15499-15502.
- 9 Tsuda, Henry & Butler, 2013. Particle transport and deposition: basic physics of particle kinetics.
10 *Comprehensive Physiology*, Volume 4, pp. 1437-1471.
- 11 Ullman & Svedmyr, 1988. Salmeterol, a new long acting inhaled beta 2 adrenoceptor agonist:
12 comparison with salbutamol in adult asthmatic patients. *Thorax*, pp. 674-678.
- 13 UNEP, 1987. *The Montreal Protocol on substances that deplete the ozone layer.*, Nairobi: UNEP.
- 14 Vankeirsbilck, et al., 2002. Applications of Raman spectroscopy in pharmaceutical analysis. *TrAC*
15 *Trends in Analytical Chemistry*, pp. 869-877.
- 16 Walkowsky & He, 2003. *Handbook of aqueous solubility data*. 1st ed. Boca Raton, FL: CRC Press.
- 17 Wang, et al., 2014. Low-frequency shift dispersive Raman spectroscopy for the analysis of respirable
18 dosage forms. *International Journal of Pharmaceutics*, Issue 469, pp. 197-205.
- 19 Wittig, Lohmann & Gmehling, 2003. Vapor–Liquid Equilibria by UNIFAC Group Contribution. 6.
20 Revision and Extension. *Industrial & Engineering Chemical Research*, 42(1), pp. 183 - 188.
- 21 Woolcock, Lundback, Ringdal & Jacques, 1996. Comparison of addition of salmeterol to inhaled
22 steroids with doubling of the dose of inhaled steroids.. *American Journal of Respiratory and Critical*
23 *Care Medicine*, pp. 1481-1488.
- 24 York & Hanna, 1994. United States of America, Patent No. US5795594 A.
- 25 Zhejiang NetSun Co., Ltd., 2010. *ChemNet.com - Global Chemical Network*. [Online]
26 Available at: <http://www.chemnet.com/cas/>
27 [Accessed 21 09 2015].
- 28
- 29